Computer-Aided: Modelled Sustainable Hybrid Catalysts for a Nano-drug Delivery System

R.L. Thage[a,*], Y. Semegni[b] § and S. Naidoo[a,*]

[a]*Department of Medicine, Division of Clinical Pharmacology, University of Stellenbosch, Western Cape, South Africa.*
[b]*Department of Mathematics, North-West University, North-West Province, Mahikeng, South Africa.*

Received 28 October 2019, revised 28 February 2020, accepted 15 April 2020.

ABSTRACT

We evaluated a hybrid catalytic power source for less invasive internal electroporation with better tissue reach than the widely used and more invasive external electroporation. We modelled how open-circuit voltage optimizes platinum-loading in catalysts to improve the electrochemical activity (ECA) possible from bioelectrogenesis through these systems and address the high costs of nano-drug delivery systems. The effects of the catalysts' convective flux and proton concentration were modelled for an enzyme (glucose oxidase) biofuel cell that was fed glucose substrate at a current rate under isothermal physiological conditions. Glucose concentrations were varied relative to anode catalyst loading models with 0.1–0.5 mg cm^{-2} platinum and alloyed (Pt-Ru-Ni) with a narrow particle size distribution. Using the free (solvation) electron model, bioelectrochemical activity (BECA) and a high open circuit voltage were generated by 5.5, 10 and 20 mM glucose with 20 kU L^{-1} glucose oxidase at 37 °C. BECA (glucose oxidase), on its own, produced pulses of various intensities for nano–microsecond durations whereas the hybrid BECA-ECA (glucose oxidase and platinum) anode catalyst provided sustainable pulses of microseconds–minute durations. Enhanced catalysis with the hybrid BECA-ECA's open circuit voltage favours compatibility of a hybrid-powered nano-drug delivery system for internal electroporation.

KEYWORDS

Catalyst optimization, platinum, alloys, free solvated electrons, hybrid fuel cell, drug delivery.

1. Introduction

Here we aimed to investigate a hybrid catalytic model (biological and metal catalysts) where the biological catalyst can enhance the anode's open circuit voltage (OCV) by supplying free (solvated) electrons and protons[1] to optimize the metal's OCV for a fuel cell, which is also a nano-drug delivery system (NDDS). We investigated two parameters as power sources for a nano-drug delivery system to simultaneously enhance drug-membrane permeation: the first one was the glucose oxidase (GOx) bioelectrochemical activity (BECA) at low glucose concentrations, and the second was a combined system, BECA electrochemical activity (ECA) model (BECA-ECA), with platinum-nanoparticle (Pt-NP) anti-microbial and anti-cancer action. We envisaged Pt having a dual function: to power an NDDS (electroporation capability) as an active nanoparticle catalyst, and as Pt^{2+}, to kill cancer and microbial cells with cytotoxicity properties. High-energy pulses might not be necessary as the cytotoxicity of Pt^{2+} would be sufficient to destroy infected cells by entering the cells through low-energy pulse electroporation. This would thus contribute to the reversible and irreversible power density needs of next generation electroporation with high-powered electric field pulses having drug-carrying capacity. Drug permeability has always been a challenging phenomenon, and carriers are known to have been used to promote drug permeation. It has been noted that the rule-of-five has a valuable set of indicators for use during permeability assessments.[2] In cases where two out of the five criteria are not met, electroporation may be able to facilitate permeability or diffusion.

1.1. The envisaged *in vivo* application was in blood containing glucose and GOx that would pass through a flow field (channel) in the NDDS with a residence time that would allow the free electrons and protons to stimulate an OCV once these were in the anode. GOx (enzyme) is a natural catalyst that helps in speeding up chemical reactions without being used or depleted during the reactions.[3] Biocatalysts (GOx enzymes) are employed in enzyme fuel cells containing anodic (oxidation) and cathodic (reduction) chambers. The overall enzymatic biological fuel cell's electrochemical activity (BECA) depends on efficient OCV generation and optimized kinetics. We hypothesize that, in the future, the hybrid-catalyst assembly will be made using the membrane electrode assembly (MEA) with layered nanoparticles and an enzyme hybrid assembly. In the assembly, proton transport will be facilitated by ionomer percolation. Currently, cancer treatment uses electroporation where the power source is applied through the skin (invasive) to destroy the affected tumour cells and to allow drug entry from the vascular system into the cell through pores induced into the cell membranes. We propose an internal (bioelectrogenesis) NDDS power source model that is also a drug (Pt^{2+}) with cytotoxic capability.

1.2. We explored a power source model, referred to as the iCAT system, to control pulse intensity for drug delivery and to facilitate reversible Type II electroporation employing a sensor-integrated NDDS. Since a fluctuation from pH 2–12 was possible inside the NDDS, a mechanism to accommodate the range is offered here, challenging the rule-of-five theories of nucleophilic attack and ionization of the drug. At 37 °C and pH 7.4, improved voltage and power density outputs were produced when compared to at pH 3 and pH 12. These results are supported by

* To whom correspondence should be addressed.
E-mail: R.L.T., lydiamaths@gmail.com / S.N., gasen.s.naidoo@gmail.com

ISSN 0379-4350 Online / ©2020 South African Chemical Institute / http://saci.co.za/journal
DOI: https://doi.org/10.17159/0379-4350/2020/v73a15

previous work showing that most biological enzymes, including glucose oxidase, have optimum activity at pH 7.4.[4] The pH-related discoveries in this study confirm that pH of a solution has an effect on the activity of an enzyme and on the ionization (oxidation or reduction of ions/loss or gain of electrons) of proteins. pH affects ionization depending on whether the enzyme's amino acid functional group is either an amino (basic) or a carboxyl (acidic) group. The pH of the matrix may positively or negatively affect the activity of an enzyme as each enzyme has an optimum pH value.[4] The operation of the Pt-NP ECA at acidic pH can keep the NDDS active not only at low pH values when the enzyme is unable to perform but also at increased pH values. In this study, it is evident that glucose, at a physiological pH of 7.4, is ideal for glucose oxidase optimization due to the power-output produced. At unlikely extremes, when in an acidic environment (acidosis) below pH 7.4 (pH 3) or above pH 7.4 (pH 12 basic/alkalosis), these conditions proved not to be favourable for glucose oxidase. This is because the ionization of amino acids in the protein caused the protein to lose electrons and the 3D structure of the protein (enzyme) to be altered and deformed; hence a lower power output was produced.

1.3. The importance of the OCV and its envisaged role in drug permeation by having electroporation support drug movement across biological membranes (BM) and bilayer lipid membranes (BLM) was closely looked at. A possible concern is that the increased medium conductivity will deform the cell and cause pore deactivation, but this can be prevented by a focussed delivery approach with targeted electroporation. Likewise, whole blood at pH 7.4 will not have sufficient $[H^+]$ to drive the required OCV; thus, the matrix will play a significant role in the supply of relevant substrates to be oxidized.

$$pH = -\log[H^+],\ [H^+] = 10\text{-}pH \text{ and } pKa = -\log Ka \qquad (1)$$

where Ka = 10-pka

Researchers[5] have reached an output of 300 μV (0.7 cm^2 surface area) that powers a drug delivery device for patients with AIDS while using whole blood glucose content as the substrate. Similarly, in our runs, we were able to optimize the power density at physiological conditions. Previous models also support development of an efficient system using validated data.[6,7]

1.4. The Pt and enzyme-layering model used the Nafion® solution and membrane as the ionomer for ion conductivity. Previously, catalyst-layering in MEAs had revealed that layers of catalyst were normally composed of carbon particles of 20–50 nm associated with the synthesis of unwanted larger particles.[5,8] We therefore avoided this by aiming for a catalytic particle size distribution (PSD) of <20 nm, supported on multi-wall carbon nano-tubes (MWCNT). The MEA containing the ionomer can interrupt the electrical conductivity and unintentionally clog the exhaust and drainage system of the MEA. This adversely affects the overpotentials and kinetics which then highlight the need for optimized MEAs with excellent conductive networks.[4,9,10] Catalyst gradients, with catalyst layers, are different in particle size or concentrations of the catalyst within the MEA, and may influence and enhance the catalyst's ECA by improving its longevity.[1,11] We therefore used high surface area MWCNTs and a narrow-alloyed nano-PSD to reduce poisoning of Pt's active sites and increase the catalyst's longevity. Our perspective is supported by models that simultaneously polarize the electric field of the extracellular matrix by using pulse efficiency to disrupt homeostasis in infected cells long enough to induce pores in the membrane. We envisage that low-intensity energy pulses with endurance capability can facilitate formation of these pores, allowing cytotoxic components of the NNDS to enter the infected cell. The extended chronoamperometry (endurance) of the NNDS is supported by the incorporation of low concentration alloys such as ruthenium and nickel (Ru and Ni) to counter the carbon dioxide and carbon monoxide poisoning in the anode and remove the ligands to release the cytotoxic Pt^{2+}. The significant rule-of-five criteria were met as the cytotoxic nanoparticles were in the <20 nm PSD range, and there was no need for the increased pore diameters that are created with high voltage during external electroporation.

2. Experimental

Our proposed power source for internal electroporation is based on a dual (hybrid) catalytic system. The two catalysts assessed here are the unsupported glucose oxidase (GOx) catalyst and the supported platinum-alloyed ruthenium and nickel (Pt-Ru-Ni/MWCNT) catalysts.

The analysis was performed in a dual cell chamber as illustrated in Fig. 1a and Fig. 1b.

The operations were controlled under physiological conditions. The temperatures were in the 26.9 °C to 37.1 °C range and pH was buffered at 7.4 with a phosphate buffer system (PBS).

2.1. Platinum Nanoparticle Synthesis

The route followed for Pt nanoparticle synthesis involved the freeze crystallization method (low temperature) for the preparation of Pt and platinum-ruthenium-nickel (Pt-Ru-Ni) on carbon,

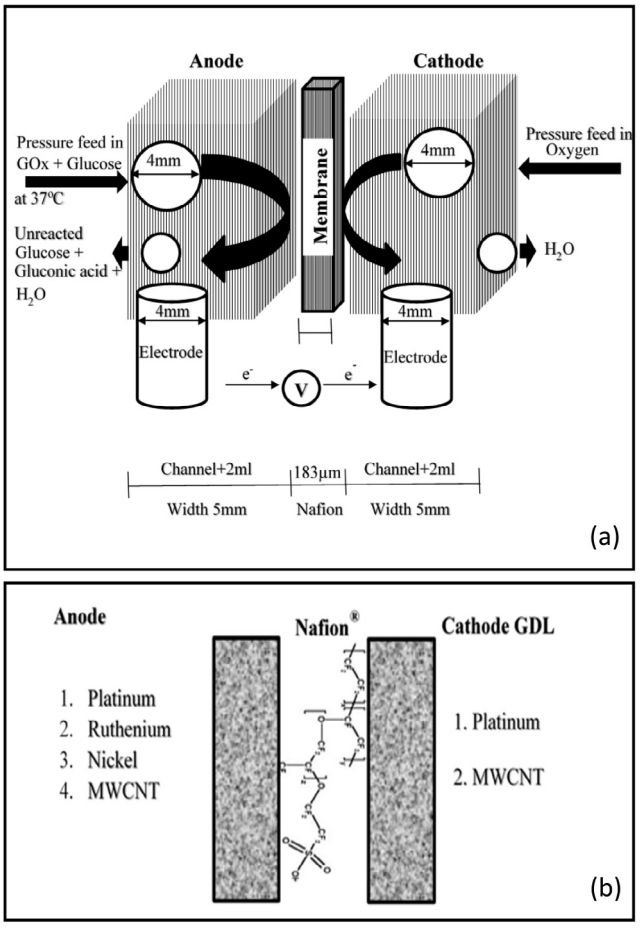

Figure 1 (**a**) Premix of glucose and GOx is pressure-fed as an unsupported GOx catalyst into the power cell (EFC) where the anode (with a carbon electrode) is in electrical contact with the cathode. (**b**) The proposed supported hybrid, containing the metal nanoparticles, and the unsupported enzyme (GOx) catalyst within an MEA.

at 4 °C, by formaldehyde reduction. This was assessed by cyclic voltammetry against commercially available Johnson Matthey® reference standards. The method involved the use of 200 mg of pre-treated carbon black on which the Pt crystals were deposited in the order that follows. The carbon black and MWCNT were initially heated at 400 °C for 5 h in an inert atmosphere. A solution containing 0.1053 g chloroplatinic acid was then added; next, the optimized nickel and ruthenium (salt precursors) for the Pt-Ru-Ni alloy were added in 100 mL 0.5 M HCl. The temperature of the solution was reduced to 4 °C (as close to 0 °C as possible). Then, 50 mL formaldehyde (40 % v/v), previously cooled to 4 °C, were added. This mixture was stirred for 1½ h at 4 °C and for 24 h overnight at room temperature. The pH was increased to 14 upon addition of 50 mL 1:1 potassium hydroxide solution. The solution was stirred at 4 °C for 5 h then heated to 85–90 °C for 20 min. The solution was filtered under vacuum then washed with 100 mL 1:1 acetic acid solution, followed by 500 mL of hot (90 °C) deionized water. It was then dried to a powder sample at 100 °C for 48 h. By varying the time, the order of precursor addition in the synthesis, the volume of the reducing agent, and the rates of addition of the reducing agent, catalytic alloyed particles of varying electronic states were synthesized.

2.2. Platinum Nanoparticle and Alloy Electrochemical Activity (ECA) Assessment

Electrochemical analysis by cyclic voltammetry was performed using a mixture (ink) of the nanoparticles with carbon support. The catalytic gel ink to be placed onto the surface of the working electrode was prepared by first weighing 8 mg of dried powder sample. To this was added 1.8 mL deionized water, then 150 μL Nafion® (5 %) solution, and the mixture was sonicated for 5 min. Next, 10 μL, as a droplet, was placed on the exposed glassy carbon electrode. This was dried to a gel-like state. Complete drying was noted as shown by visible discontinuity on the electrode's surface. Electrochemical analysis by cyclic voltammetry was done where 100 mL 0.5 M sulphuric acid was added to the test cell. The mixture was degassed by saturation with nitrogen while stirring, then a 50 mV base test was run using 0.5 M sulphuric acid. Scan cycles were run between –0.2 and 1.0 V at 20 mV s^{-1} (0.5 M sulphuric acid and 1 M methanol). Auto-Lab: Potentiostat PGSTAT 30 Eco Chemie BV, Netherlands.

2.3. Platinum and Alloy Nanoparticle Physical Morphological Study

The transmission electron microscope (TEM) and X-ray diffraction (XRD) are commonly used in the study of particle size and shape (crystallinity) of electrocatalysts. Here we used TEM to determine the physical properties of the catalysts. The XRD was used to confirm the crystallinity and lattice structures.

2.4. Model Development

Our perspective is supported with the inclusion of the hybrid enzyme's bioelectrochemical activity (GOx), Pt^{2+} and metal (alloy) heterogeneous catalysts that will improve the OCV at lower glucose concentrations than we previously reported,[9] by reducing the poisoning effect and improving catalyst endurance. The endurance and cytotoxicity testing of the metal nanoparticles will not fall within the scope of this research as it is well documented and requires experimental protocols and not data modelling. The various valences of Pt and of the metals (alloys) each have different functions and capabilities for *in vitro* assessments that will require extensive validation in future studies. Here, we focused on the use of a hybrid catalyst system with a mixed (BECA-ECA) MEA as discussed later. Also, we are only reporting on the enzyme's BECA to ensure compliance with an existing successful model. We modified a successful model developed by Jariwala and co-authors[12] to simulate our experimental data. The five compartments in the model of Jariwala *et al.* 2018,[12] were reduced to three in our modified model, namely the anodic, the cathodic and the membranous compartments as depicted in Fig. 1a.

The model's assumptions include the following:

(a) The hybrid MEA will be modelled as a single catalyst type.
(b) Anode MEA structure with mixture of the trimetallic catalysts and GOx enzyme will be used in the experimental model to fit the modelled data.
(c) Although this is a hybrid MEA structure we assume that the nanoparticles' hydrogen ion surface generation contribution is unaffected by the enzyme embedded within the MEA structure.

The chemical reactions at the cathodic and anodic compartments are, respectively:

$$\tfrac{1}{2}O_2 + H^- + 2e^- \rightarrow H_2O \quad \text{and}$$
$$C_6H_{12}O_6 + 2OH^- \rightarrow C_6H_{12}O_7 + H_2O + 2e^- \qquad (2)$$

The overall cell reaction is:

$$C_6H_{12}O_6 + \tfrac{1}{2}O_2 \rightarrow C_6H_{12}O_7 \qquad (3)$$

The transport equations at the anodic, cathodic and membranous compartments are modelled by the general mass balanced equations dictated by Fick's law, as a higher solvent–solute ratio is used.

Anodic compartment glucose transport equation ($0 < x < 5$ mm)

$$\frac{\partial C_{C_6H_{12}O_6}}{\partial t} = D^1_{C_6H_{12}O_6}\frac{\partial^2 C_{C_6H_{12}O_6}}{\partial x^2} - J\frac{\partial C_{C_6H_{12}O_6}}{\partial x} \qquad (4)$$

In this equation, $D^1_{C_6H_{12}O_6}$ represents the glucose diffusion coefficient at the cathode compartment

Membrane compartment glucose transport equation (5 mm < x < 5.183 mm)

$$\frac{\partial C_{C_6H_{12}O_6}}{\partial t} = D^2_{C_6H_{12}O_6}\frac{\partial^2 C_{C_6H_{12}O_6}}{\partial x^2} - J\frac{\partial C_{C_6H_{12}O_6}}{\partial x} \qquad (5)$$

Membrane compartment hydrogen ion transport equation

$$\frac{\partial C_{H^+}}{\partial t} = D^1_{H^+}\frac{\partial^2 C_{H^+}}{\partial x^2} - J\frac{\partial C_{H^+}}{\partial x} - D_{H^+}\frac{DV^*}{w}\frac{\partial C_{H^+}}{\partial x} \qquad (6)$$

where w is the membrane width and V* represents the dimensionless potential given by FV/RT

Cathodic compartment hydrogen ion transport equation (5.183 mm < x < 10.183 mm)

$$\frac{\partial C_{H^+}}{\partial t} = D^2_{H^+}\frac{\partial^2 C_{H^+}}{\partial x^2} - J\frac{\partial C_{H^+}}{\partial x} - K[O_2]^{1/2}\partial C_{H^+} \qquad (7)$$

The initial glucose and hydrogen ion concentrations are assumed to be 0 M throughout the system.

That is $C_{C_6H_{12}O_6}$ and $C_{H^+} = 0$ M for $0 < x < 10.183$ mm.

At $x = 0$ (left side of the anodic block)

$$C_{C_6H_{12}O_6} = C^{feed}_{C_6H_{12}O_6} \text{ and } C_{H^+} = 0 \text{ M for all } t > 0 \qquad (8)$$

At the interface of the anodic compartment ($x1 - \Delta x$) and the membrane ($x1 + \Delta x$), and similarly, at the interface of the membrane ($x2 - \Delta x$) and the cathodic compartment ($x2 + \Delta x$), the continuity conditions translate into:

$$C_{C_6H_{12}O_6}|_{x=xi-Dx} = C_{C_6H_{12}O_6}|_{x=xi+Dx} \text{ and}$$

$$C_{H^+}|_{x=xi-Dx} = C_{H^+}|_{x=xi+Dx} \quad (9)$$

for i = 1,2 and all t > 0; where x1 and x2 are the coordinates of the interfaces.

At the right boundary of the cathode compartment (x = 10.183 mm)

$$\frac{dC_{H^+}}{dx}|_{x=10.183} = 0 \text{ for all } t > 0 \quad (10)$$

The current density J is calculated at the membrane-cathode interface x = 5.183 mm as a function of the hydrogen ion concentration gradient

$$J = -F\ D_{H^+} \frac{dC_{H^+}}{dx}|_{x=5.183} \quad (11)$$

In each compartment, the interval was discretized into n = 20 sub-intervals of the same size, and the finite difference method was used to transform the partial differential equivalences into an arrangement of undeviating different equivalences, where the unknowns were the concentrations of both the glucose molecules and the protons at the various nodes of the discretized interval.

3. Results and Discussion

We explored chemical nanoparticle fuel cell (ECA) and enzymatic fuel cell (BECA) data. Our proposed model is an optimized, supported platinum-combined (alloyed) non-noble metal arrangement demonstrating hybrid-enzyme modelling of two types of electrochemical activities, BECA and ECA. The envisaged nanosecond (ns), micro-second (μs) and proposed increased pulse duration to two seconds is supported here by using the combined BECA and ECA for sustained catalytic activity that could be extended by using modified catalysis alloy combinations and anti-poisoning efficacies in surface morphology design.

3.1. MEA Free Model

The BECA monitoring in Fig. 1a was conducted at 37 °C. This supported the need for an OCV optimization by using a two-step process to supply fuel to the anode:

Step 1: A reaction between the enzyme and substrate produced the electron and protons. Electron and proton solvation occurred during preparation of the premix solution from the following reaction between glucose and glucose oxidase (Equations 2 and 3 above).

Step 2: Introduction of the premix containing the solvated electron and protons into the anode (electrochemical fuel cell), Fig. 1a, resulted in high-powered, short-duration (μs and ns) pulses.

This power surge (voltage) was mainly due to the electron and proton solvation[1] during the premix step. This is unusually high as the accumulation of electrons was due to the high concentrations of glucose and enzyme, 20 mM and 20 kU L^{-1}, respectively, which would not be possible in an MEA-type electrochemical fuel cell power density set-up. The formation of solvated (free) electron and protons is not uncommon,[1,13] and does not last very long, which means the pulses formed may be of low efficacy without the MEA support grid. Further validation of the pulse intensities will be recommended for future work. The BECA-premix freed (solvated) electrons will, however, be able to enhance the ECA OCV optimization and again, once generated by the BECA-ECA, polarize the surrounding solvent molecules (electronic and orientation);[1] this will essentially facilitate an *in vivo* matrix electric field effect for reversible electroporation. We, therefore, proposed a hybrid MEA with Pt and alloyed Ru and Ni particles to increase the power-density-capability of the hybrid electrochemical fuel cell. Sustained power was hypothesized[6] for the BECA-ECA (GOx-Pt- Ru-Ni) optimized open circuit potential.

In Fig. 2a, with a nano-range small enough to allow the flow of glucose oxidase into the proposed NDDS, the Pt-nanoparticle ECA capability, with PSD of 70 % < 10 nm, could easily accommodate an additional sustainable power source. A hybrid BECA-ECA was proposed to allow an increased packing density inside the NDDS to further support the concept of a possible 10 micrometre (μm) diameter NDDS. A reduced, narrower PSD (5–20 nm) has shown promising ECA, and the synthesis thereof was done using a freeze crystallization method. The complex nature of particle size and dissolution relationships was previously supported by researchers as well.[14,15] This method ensures a wider application where biological matrices and material are to be merged with the catalyst-holding matrices as the sub-ambient synthesis temperature is physiologically friendly. The use of hydroxy-based formulations will be beneficial to OCV optimization (increases); however, Pt can use blood contents, such as glucose, as substrates as well. The pulse potential can also aid in initiating the OCV of the Pt anode of the NDDS. The proposed hybrid's OCV results described above and below also compare the experimental and modelled catalytic efficiency of two types of catalysts. The OCV increased under the assumption that higher biological and metal catalyst concentrations will raise the ECA with greater pulse intensity since significant [H^+] increases are directly proportional to the OCV. High [H^+] was suitable for Pt nanoparticle catalysis whereas a pH level of 7 was suitable for BECA-ECA catalysis.

The proposed cumulative power hybrid BECA-ECA model with Pt-Ru-Ni alloys, Fig. 2b, contained a PSD of 70 % < 20 nm,

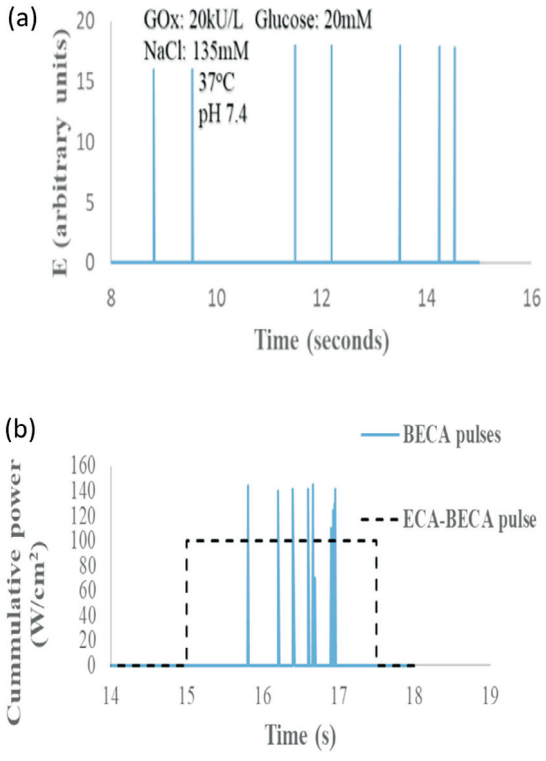

Figure 2 (**a**) BECA pulses optimized for 20 kU L^{-1} GOx at pH7.4 and 37 °C (**b**) Modelled proposed combined ECA-BECA sustained pulses compared to the high-frequency μs and ns BECA pulses

which had a significant role in producing the required polarization to ensure that the BECA supplemented the ECA. We also envisaged a more than six-fold increase for the [H^+] in the BECA-ECA model. An assembly containing 20 kU L^{-1} glucose at pH 7.4 and 135 mM sodium chloride in the anode, together with a cathode assembly containing 20 mM glucose, produced the highest power at 37 °C. The Ru ensured the longevity of the ECA by removing poisonous carbon monoxide and further supporting the sustainability of the pulse duration. An increase in enzyme concentration influenced the [H^+] and also caused an increased potential energy output; in future applications, it will facilitate an increased electric field effect. We confirmed a gradual increase in the substrate (5–10 mM) with a gradual increase in the ECA that was notably proportionate to the enzyme concentration in the reaction. The narrow PSD has shown a promising ECA, and the synthesis thereof was done using the freeze crystallization method. This method will ensure a wider application in combining heterogeneous catalysts with biological matrices and biomaterials, forming merged supramolecular biomaterials that would be otherwise damaged by other high-temperature methods of synthesis. The H^+ formation and subsequent OCV increases are promising with BECA-ECA synergies. This combined increased OCV power density will be able to support chemical (including glucose) sensor functions for the NDDS model as well. To ensure safe clearance of the NDDS the components (each less than 50 μm in diameter), these will be depleted during the functioning of the NDDS and disintegrate (supramolecular properties) after use. The remaining components will be excreted. The exciting prospect of an anti-toxicological function to reduce incidences of high-level drug and metabolite formation in the plasma matrix can be assessed in future. The use of overexpressed proteins coating the electrode and membrane in order to further enhance the hybrid system's ability to recognize and target the release of nanoparticles is recommended in future research. Future supramolecular non-covalent reversible bonding could be used to ensure a self-assembling unit.

3.2. The Membrane Electrode Assembly (MEA) Models

The combined BECA-ECA can produce increased [H^+] to facilitate an increase in direct catalytic mass activity. The significance of this effect is further supported by the BECA-ECA's sustainability where irreversible electroporation is needed.

For Figs. 3a–c, we investigated the three structures and layering arrangements for the anode MEA. We compared the power outputs from a hybrid fuel cell using a trimetallic (Pt-Ru-Ni) catalyst along with the GOx enzyme. For the arrangement shown in Fig. 3a, the GOx loading method used frequent interruptions during insertion of the enzyme layer, followed by loading of the metal catalyst, to gain the segmented (ordered) anode deposition of GOx enzyme and Pt-alloyed trimetallic catalyst. Next, for the layered arrangement, the porous layer of GOx was applied on the metallic catalyst layer. This was essentially a confirmation that electrical conductivity will be interrupted as the contact was not optimized – Fig. 3b. The ionomer's insulating effects and pore filling significance were previously noted.[16–20] As Fig. 3c shows, the model confirmed that the layers of catalyst with the larger catalytic particles fared better in the anode MEA mixture. This was because the electrical contact was easily maintained together with the ECA longevity due to larger particles (<20 nm) not dissolving, penetrating and precipitating in the membrane, as opposed to the smaller particles (<5 nm).

Factors adversely affecting conductivity include resistance at the cathode and blockage of pores with diameters less than 20 nm by the ionomer's insulation of the agglomerated Vulcan® (carbon) particles. This still occurred when the Nafion® concentration was reduced.[21] Where the ionomer's concentration exceeded half the total ink loading (>50 wt. %), the efficacy of water and gas transport was reduced. We noted the need for an efficient ionomer network promoting proton movement and optimum water and carbon monoxide (and other) exchange.[11,21, 22] We therefore used the MWCNT as supports, as they were noted to be more electrically conductive, to possess a higher surface area, and to have the engineered capability that allows gaseous exchange and molecular kinetics for mass transport. The electrically in-contact nanoparticles within the layers (Pt-Ru-Ni + GOx + ionomer) of the MEA structure provided sustained power even at higher intensities.

In Fig. 4, we show the increased H^+ generation for increasing glucose concentrations using 20 kU L^{-1} glucose oxidase at pH 7.4 and 37 °C. The MEA's structural significance in allowing the maximum substrate and catalyst active site activation was supported here:

$$H^+_s = \frac{[E][G]2k_{cat}}{[G] + k_m} \quad (12)$$

For Equation 12, both the rate coefficient of the kinetic enzyme reaction (1.6×10^3 s^{-1}) and the hydrogen ion surface generation (H^+s), (0.088 mol^{-1} m^{-2}) for the MEA were previously estimated

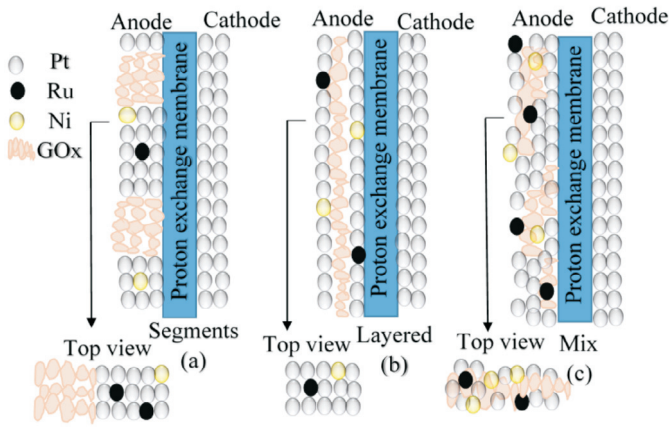

Figure 3 Anode MEA deposition structures. (**a**) Segmented ordered anode deposition of GOx enzyme and Pt-alloyed trimetallic catalyst (Pt-Ru-Ni) (**b**) layered deposition of GOx enzyme and Pt-Ru-Ni (**c**) random mixture of the Pt-Ru-Ni and GOx enzyme.

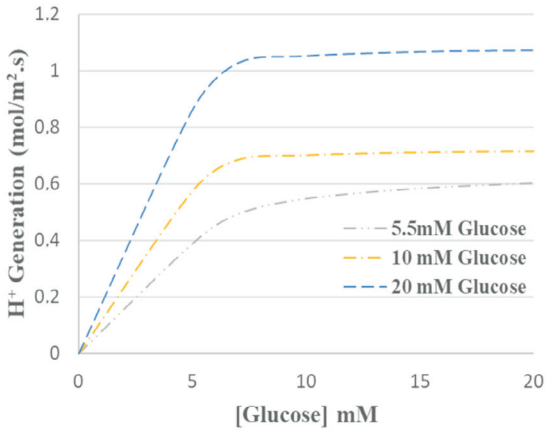

Figure 4 Modelled H^+ generation for the varied glucose concentrations for a hybrid MEA structure

by Naidoo *et al*. 2019.[23] If the power density increases by twice the value of the highest enzyme activity, the expected H^+ generation would increase from 1.1 to 2.1 mol^{-1} m^{-2} s^{-1}, and ensure a proton gradient facilitating the potential difference (Ev). Where the enzyme concentration [E] and the glucose concentration [G] were increased, there was a relative increase in the proton concentration [H^+]. This was evident for the concentration of [GO_x] as well. As the authors previously noted, [H^+] was higher at increased OCV when the H^+s was formed at the surface. The MEA containing an MWCNT support had a surface area >180 m^2 g^{-1}. Figure 4 reflects the H^+ generation for larger particles, >5 nm but <20 nm, as they showed promising stability and electrocatalytic activity. Similarly, we found that no penetration and subsequent precipitation in the membrane had occurred, confirming stability and high surface activity.[24] GOx could fill the spaces provided by the dissolved Pt and could penetrate the membrane as well. The larger particles have, however, shown improved conductivity with a higher probability of electrical contact with each other. This improved conductivity will be essential for future pulse formation and endurance. The unsupported GOx would then be a replacement of catalytic activity lost (dissolved Pt) and ensure an improvement in the OCV. The electrode porosity – for glucose entry, enzyme contact and exiting the cell – would be advantageous in a flowing system. We confirmed[24] that the smaller (<5 nm) Pt^{2+} particle count was related to the presence of unstable nanoparticles, indicating that nanoparticles larger than 5 nm were more efficient in relation to catalytic stability. The layered anode MEA, Fig. 3b, is not feasible as it causes voids and poor contact between the electrical pathways of the catalytic particles. The layered insulator effect was evident for all particle sizes tried within the structures. The MEA in Fig. 3c showed the highest combined electrochemical activity (BECA-ECA) (Fig. 5) for larger particles (>5 nm); however, the PSD with more particles in the <5 nm region, seen in Fig. 3b, showed the lowest activity (Fig. 5). This was mainly due to the poorly exposed GO_x active sites of the catalytic layer that were not in contact with glucose; it could also have resulted from the insulator effect of the ionomer and GO_x layers between the metal nanoparticles.

We compared this to a precursor premix with reduced concentration that showed much higher current. Where the modelled OCV exceeded 1.0 V, the experimental data (Fig. 5) exceeded 0.82 V as a pulse, and with shorter periods in a prototype cell configuration in an unsupported catalytic cell. It was assumed that further increases in the [H^+] can be correlated to glucose and GOx concentration increases as well as decreased potential in the lowered polarization curves (Fig. 5). The significant power density effect of H^+ surface generation and its relationship to the enzyme and substrate concentration (Fig. 5) was shown here to influence a model, allowing control of power outputs below and above the benchmark. This control is essential in establishing an electric field efficacy that would support the electrogenesis application.

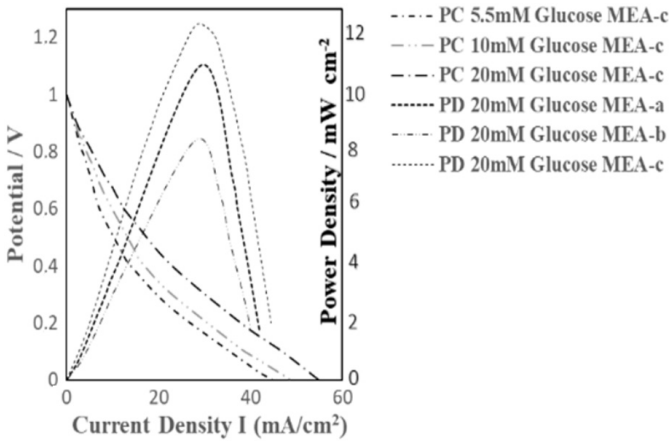

Figure 5 Experimental data curves illustrating the power densities (PD) for the three hybrid MEA structures: (**a**) segmented, (**b**) layered and (**c**) mixed. Graphs also show the polarization curves (PC) for (c), the mixed MEA structure, at 5.5, 10 and 20 mM glucose and 20 kU L^{-1} GOx.

3.3. Curve Fitting for BECA-ECA Model with Optimized OCV

Our experimental data compared well with the model by Jariwala *et al*. 2018.[12] Figure 6 below shows the comparison of modelling predictions with experimental data for MEA struc-

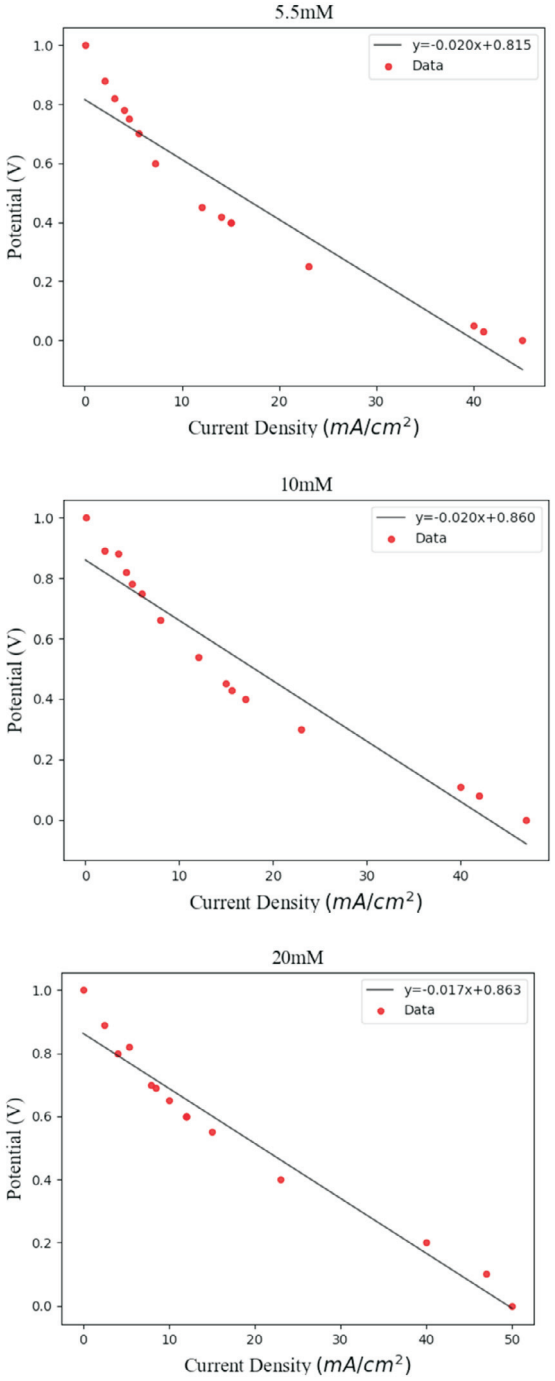

Figure 6 Matlab® was used to create models fitting the polarization curves for each of the three glucose concentrations in the mixed catalyst MEA anode structure model (**a**) 5.5 mM Glucose, (**b**) 10 mM Glucose and (**c**) 20 mM Glucose

ture (c) of Fig. 3, and the different concentrations of glucose. Here we explored the hybrid's (Enzyme - Pt-M_1-M_2/MWCNT) increased proton source capability to produce a sustainable OCV in the presence of substrates in matrices of varied pH values. An H^+ increase of 1.1 mol m^{-2} would be sufficient to allow the formation of the desired nanosecond pulses.

The experimental and modelled data in Fig. 6 focussed on sustainable power densities. This model essentially predicts outputs as the glucose and sodium chloride levels vary in the physiological matrix for the required pulse intensities. Increased BECA-ECA combined activity may result from the availability of varied substrate compositions in whole blood with increased O_2 formation and [H^+] to facilitate cell voltage polarization. The significance was shown in the compatibility where the presence of alloy nanoparticles did not adversely affect the overpotentials. Further validation is needed to confirm the actual power densities as the BECA was produced by a novel unsupported solvated GOx catalyst process that produced promising optimized power.

3.4. BECA-ECA Significance and Integration

The proposed hybrid catalyst model favoured the narrow particle size distribution. The particle size model confirmed larger 5–10 nm particles ensured electrical connectivity and endurance in the mixed MEA structures. The smaller particles, of around 2 nm, dissolved easily, forming porous areas; however, the mixed-catalyst (hybrid) arrangement, with the assistance of the multi-metallic oxide formation that increased surface activity, was better suited for ensuring electrical conductivity and structural endurance. The model assumed the BECA was enhanced by the movement of the enzyme and substrate to fill the voids caused by non-noble metal oxidation and dissolution of smaller particles. In the segmented catalyst, the GOx may have been unable to reach the voids, due to the uniform arrangement of the atoms in the pure regions. The smaller particles (<5 nm) of pure (non-hybrid) MEA showed reduced performance because of low conductivity, Pt dissolution and increased ohmic resistance in the catalyst layer. The optimized ECA used an alloyed Pt-Ru-Ni with narrowed PSD of 70 % <10 nm, and with ECA current of 8.89×10^{-3} A over a voltage range of 0.5–0.6 V in addition to a promising increased loading capability. The insertion of non-noble atoms into the crystal lattice was essential for cost reduction, structure and function optimization. The presence of nickel in the crystalline lattice structure promoted the catalytic oxidation capability of glucose and reduction of oxygen. This further enhanced the efficiency of the trimetallic catalyst. The further inhibition of hydroxide (Pt-OH_{ad}) on Pt sites by Ni may also have facilitated the charge transfer process. Ni may also have lowered the adsorption energy on Pt sites enhancing the oxidation reaction. Although we have shown significant pulse capability for reversible electroporation, further validation of the bio-catalyst (unsupported) BECA to ensure high-frequency pulse power surges is needed. High-energy pulses may not be necessary as the cytotoxicity of Pt^{2+} will be sufficient to destroy infected cells which are facilitated by low-energy pulse irreversible electroporation.

In conclusion, the BECA power sources to ensure the proposed cytotoxicity was achievable at 37 °C and shows feasibility for a next-generation implantable device application, as the NNDS no longer requires high-energy pulses to facilitate irreversible electroporation. The modelled data was representative of Pt nanoparticles and Ru/Ni alloys being useful to ensure sustainable catalysts. The atomic-scale models reveal sustainability whilst being able to optimize the pulse intensity and increased frequency. We noted that the ionomer (proton) percolation is significant in proton conductivity; whilst this should be continuous for the proton conductivity, it should not act as an insulator preventing electric conductivity of the metallic particles. The model also showed that the ionomer layer does not denature the enzyme and will be able to support the enzyme proton conduction as well as the BECA. Although a more suitable biological proton exchange membrane can be substituted in future research. The possibility of using lower substrate concentrations for the sustained catalytic OCV and proposed optimized BECA-ECA is supported here for next generation power sources in nanorobotic devices as well.

Acknowledgements

We wish to thank the NRF for their financial support. The SEM was performed at the University of Cape Town. The XRD was performed at the iThemba Labs NRF facility, in Delft in the Western Cape

Author Contributions

R.L. Thage performed the BECA experiments, designed the project and wrote the first draft using the research data. Y. Semegni developed the Matlab model and curve fitting. He also edited and contributed to the model design. S. Naidoo was the principal investigator of this NRF-funded project, contributed to the project design, revised the manuscript, and provided all the equipment, reagents, ECA, FCM and resources, including the fellowship.

§ORCID iDs

Y. Semegni: orcid.org/0000-0002-2381-6008
S. Naidoo: orcid.org/0000-0001-6676-1951

References

1 U. Schindewolf, Solvated Electron, *Adv. Chem. Ser.* **50**, 1965. American Chemical Society, Washington D.C.
2 P.D. Dobson and D.B. Kell, Carrier-mediated cellular uptake of pharmaceutical drugs: an exception or the rule? *Nat. Rev. Drug Discovery*, 2008, **7**, 205–220.
3 J. Raba and H.A. Mottola, Glucose oxidase as an analytical reagent. *Crit. Rev. Anal. Chem.*, 1995, **25**, 1–42.
4 H. Bisswanger, Enzyme assay, *Perspect. Sci.* 2014, **1**, 41–55.
5 A.K. Shukla, P. Suresh, S. Berchmans and A. Rajendran, Biological fuel cells and their applications. *Curr. Sci. India*, 2004, **87**, 455–468.
6 D. Basu and S. Basu, Mathematical modeling of overpotentials of direct glucose alkaline fuel cell and experimental validation, *J. Solid State Electrochem.*, 2013, **17**, 2927–2938.
7 R. Pathak and S. Basu, Mathematical modeling and experimental verification of direct glucose anion exchange membrane fuel cell, *Electrochim. Acta*, 2013, **113**, 42–53.
8 P. Ruzgys, M. Jakutavičiūtė, I. Šatkauskienė, K. Čepurnienė and S. Šatkauskas, Effect of electroporation medium conductivity on exogenous molecule transfer to cells *in vitro*, *Sci. Rep.*, 2019, **9**, 1436.
9 H. Yu, A. Baricci, A. Bisello, A. Casalegno, L. Guetaz, L. Bonville and R. Maric, Strategies to mitigate Pt dissolution in low Pt loading proton exchange membrane fuel cell: I. A gradient Pt particle size design, *Electrochim. Acta*, 2017, **247**, 1155–1168.
10 A. Baricci, R. Mereu, M. Messaggi, M. Zago, F. Inzoli and A. Casalegno, Application of computational fluid dynamics to the analysis of geometrical features in PEM fuel cells flow fields with the aid of impedance spectroscopy, *Appl. Energ.*, 2017, **205**, 670–682.
11 T. Soboleva, K. Malek, Z. Xie, T. Navessin and S. Holdcroft, PEMFC catalyst layers: the role of micropores and mesopores on water sorption an fuel cell activity, *ACS Appl. Mater. Inter.*, 2011, **3**, 1827–1837.
12 S. Jariwala and B. Krishnamurthy, Transport equations in an enzymatic glucose fuel cell, *Chem. Phys. Lett.*, 2018, **692**, 7–13.
13 E.J. Hart, National Standard Reference Data Series, *Act. Chim. Biol. Rad.*, 1966, **10**, 1.

14 R.K. Ahluwalia, S. Arisetty, X. Wang, R. Subbaraman, S.C. Ball, S. DeCrane and D.J. Myers, Thermodynamics and kinetics of platinum dissolution from carbon-supported electrocatalysts in aqueous media under potentiostatic and potentiodynamic conditions, *J. Electrochem. Soc.*, 2013, **160**, F447–F455.

15 E.F. Holby and D. Morgan, Application of Pt Nanoparticle dissolution and oxidation modeling to understanding degradation in PEM fuel cells, *J. Electrochem. Soc.*, 2012, **159**, B578.

16 S. Holdcroft, Fuel cell catalyst layers: a polymer science perspective, *Chem. Mater.*, 2014, **26**, 381–393.

17 M. Uchida, Y. Aoyama, N. Eda and A. Ohta, Investigation of the microstructure in the catalyst layer and effects of both perfluorosulfonate ionomer and PTFE-loaded carbon on the catalyst layer of polymer electrolyte fuel cells, *J. Electrochem. Soc.*, 1995, **142**, 4143–4149.

18 T. Soboleva, X. Zhao, K. Mallek, Z. Xie, T. Navessin and S. Holdcroft, On the micro-, meso-, and macroporous structures of polymer electrolyte membrane fuel cell catalyst layers, *ACS Appl. Mater. Interfaces*, 2010, **2**, 375–384.

19 Y. Liu, C. Ji, W. Gu, J. Jorne and H.A. Gasteiger, Effects of catalyst carbon support on proton conduction and cathode performance in PEM fuel, *J. Electro-chem. Soc.*, 2011, **158**, B614.

20 T. Soboleva, K. Malek, Z. Xie, T. Navessin and S. Holdcroft, PEMFC catalyst layers: the role of micropores and mesopores on water sorption and fuel cell activity, *ACS Appl. Mater. Interfaces*, 2011, **3**, 1827–1837.

21 S. Holdcroft, Fuel cell catalyst layers: a polymer science perspective, *Chem. Mater.*, 2014, **26**, 381–393.

22 Z. Yu, R.N. Carter and J. Zhang, Measurements of pore size distribution, porosity, effective oxygen diffusivity, and tortuosity of PEM fuel cell electrodes, *Fuel Cells*, 2012, **12**, 557–565.

23 S. Naidoo, L. Thage, Q. Ying, S. Vallie and G. Vaivars, Optimization of the enzyme power source for a nano drug delivery system fuelled by glucose in blood plasma, *IOP Conf. Ser.: Mater. Sci. Eng.*, 2013, **49** 012062.

24 A. Baricci, M. Bonanomi, H. Yu, L. Guetaz, R. Maric and A. Casalegno, Modelling analysis of low platinum polymer fuel cell degradation under voltage cycling: gradient catalyst layers with improved durability, *J. Power Sources*, 2018, **283**, 84–94.